IEEE Access
Multidisciplinary | Rapid Review | Open Access Journal

Received August 1, 2020, accepted August 23, 2020, date of publication August 28, 2020, date of current version September 10, 2020.

Digital Object Identifier 10.1109/ACCESS.2020.3020183

Implementation-Friendly and Energy-Efficient Symbol-by-Symbol Detection Scheme for IEEE 802.15.4 O-QPSK Receivers

GAOYUAN ZHANG[1,2,3], CONGYU SHI[1], CONGZHENG HAN[2], XINGWANG LI[4], (Senior Member, IEEE), DAN WANG[1], KHALED RABIE[5], (Senior Member, IEEE), AND RUPAK KHAREL[6], (Senior Member, IEEE)

[1]School of Information Engineering, Henan University of Science and Technology, Luoyang 471023, China
[2]Key Laboratory of Middle Atmosphere and Global Environment Observation, Institute of Atmospheric Physics, Chinese Academy of Sciences, Beijing 100029, China
[3]School of Aeronautics and Astronautics, University of Electronic Science and Technology of China, Chengdu 610054, China
[4]School of Physics and Electronic Information Engineering, Henan Polytechnic University, Jiaozuo 454000, China
[5]Department of Engineering, Manchester Metropolitan University, Manchester M15 6BH, U.K.
[6]Department of Computing and Mathematics, Manchester Metropolitan University, Manchester M15 6BH, U.K.

Corresponding authors: Gaoyuan Zhang (zhanggaoyuan407@163.com), Congzheng Han (c.han@mail.iap.ac.cn), and Dan Wang (wangdaniel2004@163.com)

This work was supported in part by the National Natural Science Foundation of China under Grant 61701172, Grant 41605122, Grant 61701059, Grant 61701062, Grant 61801170, Grant 61801171, and Grant 61772175; in part by the Scientific and Technological Innovation Team of Colleges and Universities in Henan Province under Grant 20IRTSTHN018; in part by the Open Foundation of the Key Laboratory of Middle Atmosphere and Global Environment Observation, Institute of Atmospheric Physics, Chinese Academy of Sciences; in part by the Postdoctoral Science Foundation, University of Electronic Science and Technology of China, under Grant Y02006023601721; in part by the Program for Everest Scholar Talents Development in Tibet University; and in part by the Program for Science and Technology Innovation Talents in the University of Henan Province (Educational Committee) under Grant 17HASTIT025.

ABSTRACT In this article, the noncoherent detection scheme for the receiver in wireless sensor nodes is discussed. That is, an implementation-friendly and energy-efficient symbol-by-symbol detection scheme for IEEE 802.15.4 offset-quadrature phase shift keying (O-QPSK) receivers is investigated under both pure additive white Gaussian noise (AWGN) channel and fading channel. Specifically, the residual carrier frequency offset (CFO) of the chip sample is estimated and compensated with the aid of the preamble; then, the standard noncoherent detection scheme with perfectly known CFO is directly configured. The corresponding simulation results show that only 4 preamble symbols is sufficient for accurate CFO estimation. Compared with the conventional noncoherent detector, the average running time per data packet of our enhanced detector is only 0.17 times of the former; meanwhile, at the packet error rate of 1×10^{-3}, our enhanced detector can obtain 2.2 dB gains in the (32, 4) direct sequence spread spectrum system. A more reasonable trade-off between complexity and reliability is thus achieved for energy-saving and maximum service life in wireless sensor networks (WSNs).

INDEX TERMS Internet of Things, IEEE 802.15.4 wireless sensor networks, offset QPSK, symbol-by-symbol detection.

I. INTRODUCTION

Recently, wireless sensor networks (WSNs) has received a great deal of attention form diverse fields, particularly because of its important role in the ''edge access'' of the 5G-enabled ''Internet of Things (IoT)'' [1]–[3]. Compared with traditional wireless networks, pervasive WSNs pay more attention to energy-saving and cost effectiveness. Thus, the IEEE 802.15.4 standard [4], [5], which is tailored for low-speed and ubiquitous communication between inexpensive devices, has been widely applied in WSNs and shown tremendous potential for development of 5G-enabled IoT [6].

The associate editor coordinating the review of this manuscript and approving it for publication was Yassine Maleh.

The reliability of WSNs is one of the most important factors, which may limit the application depth and width [7], [8]. Clearly, the detection performance of the receiver is closely related to the throughput and energy efficiency of the wireless sensor node, and even directly affects the transmission efficiency of the whole WSNs [9]–[12]. In this work, we investigate this issue from the perspective of receiver detection mechanism, which is extremely significant for academics and end-users as well.

According to the IEEE 802.15.4 standard, the offset quadrature phase shift keying (O-QPSK) direct sequence spread spectrum (DSSS) scheme is required in 780/868/915/2380/2450 MHz frequency band [4], [5]. The high spectral efficiency as well as constant envelope are attractive characteristics for O-QPSK modulation, which makes it be extensively applied in code division multiple access systems, satellite communications and so on [13]. Generally, the coherent detection scheme exhibits excellent performance because the carrier synchronization is considered to be perfectly achieved at the receiver. However, it is not suitable for battery-powered WSNs. This stems from the fact that its performance completely depends on perfect estimation of carrier phase offset (CPO), which is clearly a high-complexity as well as energy-intensive process [14]. Therefore, the noncoherent detection scheme, wherein the carrier synchronization is not required at the receiver, is an attractive alternative for energy-efficient WSNs.

In recent years, a variety of noncoherent detection schemes for IEEE 802.15.4 O-QPSK receivers have been proposed. The main related work is as follows. Based on the maximum likelihood (ML) criteria, D. Park and S. Park proposed a low-complexity decision-assisted scheme [15], [16], yet there is an inevitable temporary error propagation. The work of S. C. Dai *et al.* introduced a novel scheme utilizing the correlation between adjacent pseudo noise chip signals [17], which exhibits excellent performance, especially high robustness to both phase and frequency offset. C. Wang *et al.* considered an additive decision metric to implement symbol-level differential coherence detection scheme in [18], which achieved a certain degree of performance improvement at the expense of complexity increment. With the aid of the preamble to deal with unknown carrier frequency offset (CFO), J. H. Do *et al.* proposed a coherent detection-based scheme [19]. Yet, this scheme still has high complexity, which is mainly because of the multiplication and trigonometric operations (*i.e.*, sine and cosine). Furthermore, the receiver was synchronized by using cross-correlation and auto-correlation operation in [20], which is actually complicated and energy-consuming. Therefore, it is imperative to develop compatible and low-complexity CFO estimation schemes for O-QPSK noncoherent detection schemes in IEEE 802.15.4 WSNs.

Due to Doppler shift and/or the oscillator variation of the transmitter and receiver, there is an inevitable deviation between the transmitted and received carrier signals. J. Y. Oh *et al.* indicated that initial phase mismatch and the CFO will lead to a significant performance degradation. Hence, it is necessary to implement CFO estimation and compensation at the receiver [21]. The related work of CFO estimation is as follows. Bloch *et al.* proposed a powerful full estimation scheme in [22]. Yet, it's not affordable in wireless sensor, since the inverse tangent operation is too complicated to be implemented. Considering the mathematical approximation $\tan^{-1}x \approx 0$, Lee *et al.* firstly simplified this complete estimation, wherein the CFO was quantified by four constant phases [23]. Unsurprisingly, Zhang *et al*. considered more desirable approximation, *i.e.*, $\tan^{-1}x \approx x$ [24]. In this context, the observation interval is subdivided into four equiangular regions, and an adaptive offset adjustment term is designed to compensate the estimation error in [23]. However, the non-linear operation is still inevitable. [25] introduce a simplified estimation scheme with only linear operation, which adopts the approximation $\sin^{-1}x \approx x$ [22].

In this work, we propose an implementation-friendly and energy-efficient symbol-by-symbol detection scheme for IEEE 802.15.4 O-QPSK receivers. Unlike the conventional receiver, where complexity-intensive detector and/or estimator are equipped, we turn our main attention towards the simple design of detection and estimation schemes to achieve further balance between implementation complexity and detection reliability. The main contributions are as follows:

- Previous studies have assumed that the amplitude of the signal is not affected by the channel, that is, fading is not considered. In this work, we consider the more general case and study the receiver under both slow fading and pure additive white Gaussian noise (AWGN) channels.
- A new detection scheme is proposed, where the complexity-intensive and time-consuming chip-delay operation is not involved. Preamble-assisted and implementation-friendly estimator is also given to further reduce the complexity, where however the performance requirements of the IEEE 802.15.4 protocol is still satisfied.
- The detection characteristic of the receiver is investigated from numerous aspects through comprehensive simulation. Specially, in order to verify the robustness of our receiver to the CPO, the detection results in presence of random varying CPO are studied.

The remaining structures of this article are as follows. In Section II, we introduce the signal model. Section III briefly goes over the conventional noncoherent and coherent-based detection schemes. Section IV concentrates on our proposed enhanced detection scheme in detail. In Section V, the numerical results and discussion are presented. Finally, in Section VI, some conclusions and future work are offered.

II. SIGNAL MODEL

According to IEEE 802.15.4 standard [4], the O-QPSK physical layer (PHY) uses hexadecimal quasi-orthogonal modulation. The specific data process is shown in Fig. 1. Here

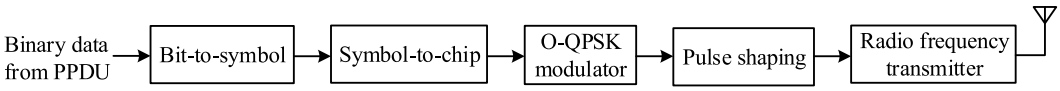

FIGURE 1. The physical layer data transmission process in the IEEE 802.15.4 WSNs.

4-bit data is employed to choose one of 16 quasi-orthogonal pseudo-noise (PN) sequences. In particular, the analysis in this work are all based on the (32, 4)-DSSS system, wherein each symbol is spread into 32 chips. For more details of the mapping rule, the readers can refer to Table 2 in [19]. Note that, (16, 4)-DSSS and (8, 4)-DSSS schemes are also provided in [4]. All of the results achieved in this work can be easily tailored to the system with these two mapping schemes, which however is not given here except for detection performance analysis in Section V-B and V-C.

Considering ideal carrier synchronization at the receiver, we select a more general signal model. For the mth symbol $E[m]$, its complex base-band received chip sequence is as follows:

$$r_{m,k} = h_{m,k} s_{m,k} e^{j(\omega_{m,k} k T_c + \theta_{m,k})} + \eta_{m,k}, \quad 1 \le k \le K/2. \tag{1}$$

Here, $h_{m,k}$ denotes the multiplicative fading. $s_{m,k}$ is the kth transmitted bipolar O-QPSK modulation chip in the mth symbol interval. $\omega_{m,k} = 2\pi f_{m,k}$ and $\theta_{m,k}$ are the CFO and CPO in radian, respectively. T_c is the chip period. $\eta_{m,k}$ is a complex AWGN with zero-mean and known variance $N_0/2$. K is the length of PN sequence, $K = 32$ in (32, 4)-DSSS system and $K = 16$ in (16, 4)-DSSS system.

In order to describe the estimation and detection scheme in a more general form, this work considers the slow fading channel, which is characterized by a random variable $h_{m,k}$ with Rayleigh distribution. We assume that the $h_{m,k}$, CFO $\omega_{m,k}$, CPO $\theta_{m,k}$ are unknown and random but constant across a packet transmission, that is $h_{m,k} = h$, $\omega_{m,k} = \omega$, $\theta_{m,k} = \theta$ and $\eta_{m,k} = \eta$.

III. THE CONVENTIONAL NONCOHERENT AND COHERENT-BASED DETECTION SCHEMES

According to the IEEE 802.15.4 standard, in 2.4GHz frequency band, the maximum carrier frequency is 2.48GHz and the transmitted CFO shall be up to is ±40 ppm ("ppm" means parts per million, *i.e.*, ±99.2KHz). Then, the worst-case CFO is ±80 ppm (*i.e.*, ±198.4KHz), corresponding to +40ppm CFO in the transmitter and −40ppm CFO in the receiver.

In order to achieve the required reliability in a high-frequency-variant environment, various schemes have been proposed. The two representative ones are the conventional noncoherent detection scheme and its improved strategy (*i.e.*, the coherent detection-based scheme) [19]. The former uses chip-level differential filter, while the latter is with the aid of frequency offset estimator.

A. THE CONVENTIONAL NONCOHERENT DETECTION SCHEME

As shown in [19], in conventional detection-based scheme, carrier frequency offset effect (CFOE) is eliminated by the square operation. The specific implementation process for this scheme are as follows.

First, the received chip sample sequence after the matched filter is respectively subjected to $1T_c$, $2T_c$, and $3T_c$ chip delay differential filter. The filter output $A_{m,k-N}$ is

$$\begin{aligned} A_{m,k-N} &= r_{m,k} r^*_{m,k-N} \\ &= |h|^2 s_{m,k} s^*_{m,k-N} e^{j\omega N T_c} + \eta(0), \\ &\quad N+1 \le k \le L_1. \end{aligned} \tag{2}$$

Here, N is the number of the delayed chip sample, and $N \in \{1, 2, 3\}$. L_1 is referred to as the sample number for each symbol, and $N+1 \le L_1 \le K/2$. $\eta(0)$ is the integrated noise term. We can see that the time-varying CFOE component $\omega k T_c$ embedded in the chip sample $r_{m,k}$ is now converted into a constant value $\omega N T_c$ in $A_{m,k-N}$. The 16 differential PN sequences are expressed as

$$B_{n,k-N} = s_{n,k} s^*_{n,k-N}, \quad 0 \le n \le 15,\ N+1 \le k \le L_1. \tag{3}$$

where the superscript $*$ represents a complex conjugate operation.

Then, the cross-correlation operation is performed between the the multi-delay differential filter output $\{A_{m,k-N}\}$ and the differential PN sequence $\{B_{n,k-N}\}$. After envelope detection and accumulation, we arrive at the decision metric

$$V_{m,n} = \left| \sum_{N=1}^{3} \sum_{k=N+1}^{L_1} A_{m,k-N} B^*_{n,k-N} \right|^2. \tag{4}$$

Finally, by demapping V_m, the bit information $E[m]$ is obtained. Here, the final decision metric V_m is given by

$$V_m = \arg\max_{0 \le n \le 15} \{V_{m,n}\}. \tag{5}$$

This detection scheme directly borrows the idea in [6]. Note however that the CFO and spectrum spread are not involved in [6]. Its main advantage is that the receiver avoids the estimation operation. It is just for this reason that it has significantly performance degradation. There is a slight difference between the schemes given in [19] and this work. Here, the CPO as well as fading is further considered, while it is not the case in [19]. Thus, we summarize the detailed process of our conventional noncoherent detection scheme in Algorithm 1.

Algorithm 1: The Conventional Noncoherent Detection Algorithm

Input: $r_{m,k}$: baseband samples of the mth symbol period $E[m]$;
L: payload length of the physical layer protocol data unit (PPDU) (here, $L = 176$ bits, *i.e.* 44 symbols);
L_1: sample number for each symbol of the actual data, and $N+1 \le L_1 \le K/2$;
K: chip length of the pseudo-random sequence (PN), and $K = 32$;
N: the number of differential chip, and $N \in \{1, 2, 3\}$.
Output: $\{\widehat{E}[m]\}$: the actual bit data.

Initialize $L = 176$, $K = 32$, and $V_m = 0$;
for $N = 1;\ 1 \le N \le 3;\ N++$ **do**
  for $m = 1;\ m \le L/4;\ m++$ **do**
    for $k = N+1;\ k \le L_1;\ k++$ **do**
      $A_{m,k-N} \leftarrow r_{m,k} r^*_{m,k-N}$;
    end
  end
  for $n = 0;\ n \le 15;\ n++$ **do**
    for $k = N+1;\ k \le L_1;\ k++$ **do**
      $B_{n,k-N} \leftarrow s_{n,k} s^*_{n,k-N}$;
    end
  end
end
for $m = 1;\ m \le L/4;\ m++$ **do**
  for $n = 0;\ n \le 15;\ n++$ **do**
    for $N = 1;\ N \le 3;\ n++$ **do**
      for $k = N+1;\ k \le L_1;\ k++$ **do**
        $V_{m,n} \leftarrow V_{m,n} + A_{m,k-N} B^*_{n,k-N}$;
      end
    end
    $V_{m,n} \leftarrow |V_{m,n}|^2$;
    if $V_m \le V_{m,n}$ **then**
      $V_m \leftarrow V_{m,n}$
    end
  end
end
Obtain the bit detection information $\{\widehat{E}[m]\}$ by demapping the output value of the comparator $\{V_m\}$;
return $\{\widehat{E}[m]\}$.

B. THE COHERENT DETECTION-BASED SCHEME

To reducing the performance degradation, J. H. Do *et al.* proposed a coherent detection-based scheme, which only considers CFO as shown in (2) of [19]. However, we considers both CFO and CPO as shown in (1). Algorithm 2 shows the implementation process, and the detailed steps are as follows.

First, similar to the conventional noncoherent detection scheme, the differential signals $A_{m,k-N}$ and differential PN sequences $B_{n,k-N}$ shown in (2) and (3) can be obtained.

Algorithm 2: The Coherent Detection-Based Algorithm

Input: $r_{m,k}$: baseband samples of the mth symbol period $E[m]$;
L: payload length of the PPDU (here, $L = 176$ bits, *i.e.* 44 symbols);
L_1: sample number for each symbol, and $N+1 \le L_1 \le K/2$;
L_2: sample number for the mth symbol of the preamble, and $N+1 \le L_2 \le K/2$;
K: chip length of the pseudo-random sequence (PN), and $K = 32$;
N: the number of differential chip, and $N \in \{1, 2, 3\}$;
J_1: the length of preamble, and $1 \le J_1 \le J$, where $J = 8$ is the maximum length.
Output: $\{\widehat{E}[m]\}$: the actual bit data.

Initialize $L = 176$, $K = 32$, and $Z_m = 0$;
for $N = 1;\ 1 \le N \le 3;\ N++$ **do**
  for $k = N+1;\ k \le L_2;\ k++$ **do**
    $B_{0,k-N} \leftarrow s_{0,k} s^*_{0,k-N}$;
  end
  for $m = 1;\ m \le J_1;\ m++$ **do**
    for $k = N+1;\ k \le L_2;\ k++$ **do**
      $A_{m,k-N} \leftarrow r_{m,k} r^*_{m,k-N}$;
      $f_{est} \leftarrow f_{est} + A_{m,k-N} B^*_{0,k-N}$;
    end
  end
  $f_{est} \leftarrow f_{est}/J_1\,(L_2 - N)$;
end
for $m = J_1 + 1;\ m \le J_1 + L/4;\ m++$ **do**
  for $n = 0;\ n \le 15;\ n++$ **do**
    for $N = 1;\ N \le 3;\ n++$ **do**
      for $k = N+1;\ k \le L_1;\ k++$ **do**
        $Z_{m,n} \leftarrow Z_{m,n} + A_{m,k-N} B^*_{n,k-N} f^*_{est}$;
      end
    end
    $Z_{m,n} \leftarrow Re\,(Z_{m,n})$;
    if $Z_m \le Z_{m,n}$ **then**
      $Z_m \leftarrow Z_{m,n}$
    end
  end
end
Obtain the bit detection information $\{\widehat{E}[m]\}$ by demapping the output value of the comparator $\{V_m\}$;
return $\{\widehat{E}[m]\}$.

Then, the delay differential operation is carried out on the bipolar PN sequence and the received chip sequence for the preamble symbol. We can obtain the complex expressions $A_{m,k-N}$ and $B_{0,k-N}$ as follows.

$$\begin{aligned} A_{m,k-N} &= r_{m,k} r^*_{m,k-N} \\ &= |h|^2 s_{m,k} s^*_{m,k-N} e^{j\omega N T_c} + \eta\,(1)\,, \end{aligned}$$

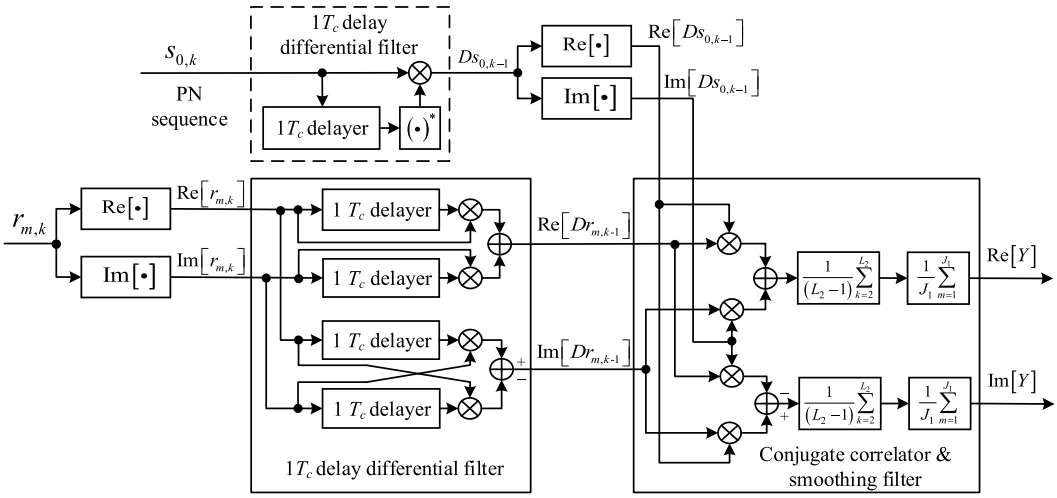

FIGURE 2. The structure of frequency offset measurement Y.

$$1 \le m \le J_1, \quad N+1 \le k \le L_2. \tag{6}$$

$$B_{0,k-N} = s_{0,k} s^*_{0,k-N}, \quad N+1 \le k \le L_2. \tag{7}$$

Here, J_1 is the observation length of the preamble symbol, and $1 \le J_1 \le J$, where $J = 8$ is the maximum preamble length. L_2 is the sample number for the mth symbol of the preamble, and $N+1 \le L_2 \le K/2$. $\{s_{0,k}\}$ is the first bipolar spreading sequence. $\eta(1)$ represents an integrated noise component. Note that, unless otherwise specified, the maximum preamble length is considered in this work, which is $J_1 = 8$.

Further, the frequency offset estimator is obtained by using the correlation between the preamble symbol and the PN sequence as

$$\begin{aligned} f_{est} &= \frac{1}{J_1 (L_2 - N)} \sum_{m=1}^{J_1} \sum_{k=N+1}^{L_2} A_{m,k-N} B^*_{0,k-N} \\ &= |h|^2 e^{j\omega N T_c} + v \\ &= |f_{est}| \left[\cos\left(\widehat{\omega N T_c}\right) + j \sin\left(\widehat{\omega N T_c}\right) \right], \end{aligned} \tag{8}$$

where v is set as an integrated noise term.

Next, a post-compensation operation is performed, and the combiner output of this detection scheme can be obtained as follows.

$$Z_{m,n} = Re\left(\sum_{N=1}^{3} \sum_{k=N+1}^{L_1} A_{m,k-N} B^*_{n,k-N} f^*_{est} \right), \tag{9}$$

where $Re\{x\}$ represents the real part of x. L_1 is the sample number for each symbol, and $N+1 \le L_1 \le K/2$.

Finally, the maximum of 16 symbols is selected as the output of maximum value selector.

$$Z_m = \arg\max_{0 \le n \le 15} \{Z_{m,n}\}. \tag{10}$$

After demapping, the final data $E[m]$ can be obtained. Yet, the receiver is still high-complexity receiver, which is mainly due to the complicated delay difference operation and correlation operation of the estimator f_{est}. For more details of the receiver structure, please refer to Figs. 4 and 5 in reference [19].

IV. THE PROPOSED NONCOHERENT DETECTION SCHEME

In view of the high implementation complexity and the drawback of post-compensation of these existing schemes, based on a heuristic idea, this work introduces an implementation-friendly and energy-efficient symbol-by-symbol detection scheme for IEEE 802.15.4 O-QPSK receivers. Specifically, there is no need to acquire the prior knowledge of the initial phase and CFO. The specific implementation process is detailed below.

Firstly, as shown in Fig. 2, the correlation and accumulation operation between the complex baseband received signal of the preamble and the PN sequence is performed, and the measurement Y can be acquired by

$$\begin{aligned} Y &= \frac{1}{J_1 (L_2 - 1)} \sum_{m=1}^{J_1} \sum_{k=2}^{L_2} Dr_{m,k-1} Ds^*_{0,k-1} \\ &= |h|^2 e^{j\omega T_c} + \lambda. \end{aligned} \tag{11}$$

Here, J_1 represents the preamble length, and $1 \le J_1 \le J$, wherein $J = 8$ is the maximum length of preamble. L_2 is the sample number for the mth symbol of the preamble, and $2 \le L_2 \le K/2$. λ is an integrated noise term. Note that, for simplifying the detection process, only the $1T_c$ chip delay difference is considered here, *i.e.*, $N = 1$. The complex baseband received signal $Dr_{m,k-1}$ corresponding to the preamble and $Ds_{0,k-1}$ corresponding to the PN sequence are respectively expressed as follows:

$$\begin{aligned} Dr_{m,k-1} &= r_{m,k} r^*_{m,k-1} \\ &= |h|^2 s_{m,k} s^*_{m,k-1} e^{j\omega T_c} + N_{m,k}, \\ & \quad 1 \le m \le J_1, \quad 2 \le k \le L_2. \end{aligned} \tag{12}$$

$$Ds_{0,k-1} = s_{0,k}s^{*}_{0,k-1}, \quad 1 \le k \le L_2. \tag{13}$$

In the 2.4 GHz PHY of the IEEE 802.15.4 O-QPSK receiver, the preamble "0000" is mapped into the first of 16 PN sequences. $N_{m,k}$ is an integrated noise component. The structural diagram of measurement Y is exhibited in Fig. 2.

Next, utilizing the measurement Y shown in (11), we can acquire a quantization function $g(Y)$ representing an estimator of the frequency. Hence, the CFOE can be intuitively estimated.

$$\widehat{\varphi} \triangleq \omega Tc = g(Y). \tag{14}$$

Due to different estimation algorithms, the estimator $\widehat{\varphi}$ have different representation forms.

A. FULL ESTIMATOR

We first introduce the full estimator in (15).

$$\widehat{\varphi} = \angle Y = \begin{cases} tan^{-1}\left(\dfrac{Im(Y)}{Re(Y)}\right), \\ if\ Re(Y) > 0 \\ \dfrac{\pi}{2}, \\ if\ Re(Y) = 0\ and\ Im(Y) \ge 0 \\ -\pi - tan^{-1}\left(\dfrac{Im(Y)}{Re(Y)}\right), \\ if\ Re(Y) < 0 \\ -\dfrac{\pi}{2}, \\ if\ Re(Y) = 0\ and\ Im(Y) < 0. \end{cases} \tag{15}$$

Here, the constant term, *i.e.*, $0, \pi/2, -\pi$, and $-\pi/2$, is called as the coarse estimation, and $Re(Y)$ and $Im(Y)$ represent the real and imaginary part of Y respectively.

B. SIMPLIFIED ESTIMATOR WITH $\tan^{-1}x$ FORM

Further, Zhang *et al.* [24] subdivide the complex observation space into four equiangular sectors as shown in (16), which are same as the four regions shown in Table 1 of [23]. They can be distinguished from each other by only simply comparing measurement magnitudes and signs of Y.

$$\widehat{\varphi} = \begin{cases} tan^{-1}\left(\dfrac{Im(Y)}{Re(Y)}\right), \\ if\ Re(Y) > 0\, and\ |Re(Y)| \ge |Im(Y)| \\ \dfrac{\pi}{2} - tan^{-1}\left(\dfrac{Re(Y)}{Im(Y)}\right), \\ if\ Im(Y) > 0\, and\ |Re(Y)| < |Im(Y)| \\ -\pi + tan^{-1}\left(\dfrac{Im(Y)}{Re(Y)}\right), \\ if\ Re(Y) < 0\, and\ |Re(Y)| \ge |Im(Y)| \\ -\dfrac{\pi}{2} - tan^{-1}\left(\dfrac{Re(Y)}{Im(Y)}\right) \\ if\ Im(Y) < 0\, and\ |Re(Y)| < |Im(Y)|. \end{cases} \tag{16}$$

TABLE 1. Parameters used in simulations.

Parameter	Detailed Description
Channel condition	pure AWGN and slow Rayleigh fading
Power of the complex noise	1/SNR
Detection scheme	Chip-level noncoherent
Compensation scheme	Precompensation
Timing synchronization	Perfect
Data modulation	Offset QPSK
Symbols	16-ary quasi-orthogonal
Payload length of PSDU (bits)	176
Spreading factor	32 or 16
Chip rate (Mchip/s)	2
Symbol rate (ks/s)	62.5
Binary data rate (kb/s)	250
Carrier frequency (MHz)	2480
CPO θ (rads)	Uniform distribution in $(-\pi, \pi)$
CFO f (ppm)	Symmetrical triangular distribution in (-80, 80)
PN length K	32 or 16
preamble length L	8
Computer version	Win10_64 bit
Computer central processing unit (CPU)	Intel Core i5-4210U 2.40GHz

We observe immediately from (15) and (16) that the arctan operation is inevitable. High computational complexity and are unreasonable in the IEEE 802.15.4 wireless sensor network receiver, where low power and low cost are the most important design indicators. Considering that $|Re(Y)/Im(Y)|$ or $|Im(Y)/Re(Y)|$ is not more than 1 and is independent in CFO estimation and signal-to-noise ratio (SNR) condition, we can directly adopt the mathematical approximation $\tan^{-1}x \approx x$ for (17) without unnecessary calculation errors. That is, (16) can be expressed as

$$\widehat{\varphi} \approx \begin{cases} \dfrac{Im(Y)}{Re(Y)}, \\ if\ Re(Y) > 0\, and\ |Re(Y)| \ge |Im(Y)| \\ \dfrac{\pi}{2} - \dfrac{Re(Y)}{Im(Y)}, \\ if\ Im(Y) > 0\, and\ |Re(Y)| < |Im(Y)| \\ -\pi + \dfrac{Im(Y)}{Re(Y)}, \\ if\ Re(Y) < 0\, and\ |Re(Y)| \ge |Im(Y)| \\ -\dfrac{\pi}{2} - \dfrac{Re(Y)}{Im(Y)}, \\ if\ Im(Y) < 0\, and\ |Re(Y)| < |Im(Y)|. \end{cases} \tag{17}$$

Obviously, compared with the CFO estimation scheme in (15) and the space subdivision method, our adaptive CFO estimation scheme in (17) possesses simple rules for space division and friendly uses the triangular approximation $\tan^{-1}(x) \approx x$ and $\sin^{-1}(x) \approx x$ without undesired error.

C. SIMPLIFIED ESTIMATOR WITH $\sin^{-1}x$ FORM

Similarly, combining the observation interval division rules in [24], $\widehat{\varphi}$ can also be expressed by the $\sin^{-1}x$ form as shown

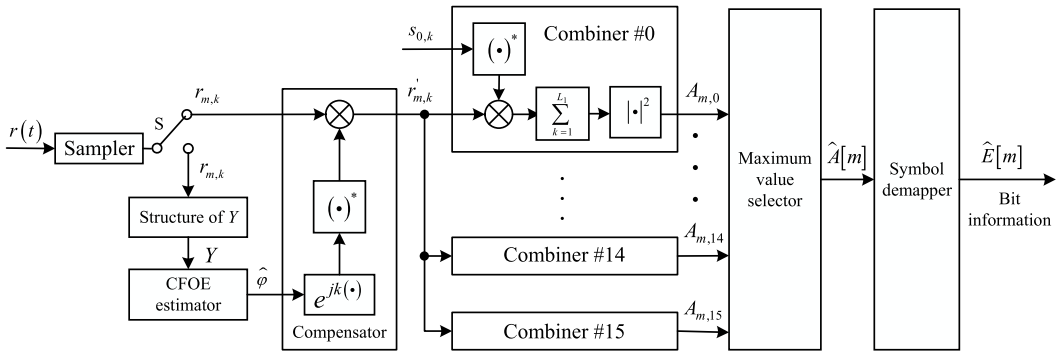

FIGURE 3. The structure of the proposed receiver.

in (18).

$$\widehat{\varphi} = \begin{cases} sin^{-1}\left(\dfrac{Im\,(Y)}{\sqrt{Re^2\,(Y)+Im^2\,(Y)}}\right), \\ if\ \ Re\,(Y) > 0\ and\ \ |Re\,(Y)| \geq |Im\,(Y)| \\ \dfrac{\pi}{2} - sin^{-1}\left(\dfrac{Re\,(Y)}{\sqrt{Re^2\,(Y)+Im^2\,(Y)}}\right), \\ if\ Im\,(Y) > 0\ and\ \ |Re\,(Y)| < |Im\,(Y)| \\ -\pi - sin^{-1}\left(\dfrac{Im\,(Y)}{\sqrt{Re^2\,(Y)+Im^2\,(Y)}}\right), \\ if\ \ Re\,(Y) < 0\ and\ \ |Re\,(Y)| \geq |Im\,(Y)| \\ \dfrac{\pi}{2} + sin^{-1}\left(\dfrac{Re\,(Y)}{\sqrt{Re^2\,(Y)+Im^2\,(Y)}}\right), \\ if\ Im\,(Y) < 0\ and\ \ |Re\,(Y)| < |Im\,(Y)|\,. \end{cases} \tag{18}$$

Assuming a high SNR over the AWGN with perfect CSI, and the non-Gaussian noise term in (11) is small enough, we get

$$\begin{aligned} \sqrt{Re^2\,(Y)+Im^2\,(Y)} = |Y| &= \left||h|^2 e^{j\omega T_c} + \lambda\right| \\ &\approx |h|^2 = 1. \end{aligned} \tag{19}$$

Then, with trigonometric approximation $\sin^{-1}x \approx x$ and substituting (19) into (18), another simplified estimator $\hat{\varphi}$ can be obtained as given by (20).

$$\widehat{\varphi} \approx \begin{cases} Im\,(Y)\,, \\ if\ \ Re\,(Y) > 0\ and\ \ |Re\,(Y)| \geq |Im\,(Y)| \\ \dfrac{\pi}{2} - Re\,(Y)\,, \\ if\ Im\,(Y) > 0\ and\ \ |Re\,(Y)| < |Im\,(Y)| \\ -\pi - Im\,(Y)\,, \\ if\ \ Re\,(Y) < 0\ and\ \ |Re\,(Y)| \geq |Im\,(Y)| \\ -\dfrac{\pi}{2} + Re\,(Y)\,, \\ if\ Im\,(Y) < 0\ and\ \ |Re\,(Y)| < |Im\,(Y)|\,. \end{cases} \tag{20}$$

Furthermore, for slow fading channel, we have

$$\begin{aligned} \sqrt{Re^2\,(Y)+Im^2\,(Y)} = |Y| &= \left||h|^2 e^{j\omega T_c} + \lambda\right| \\ &\approx |h|^2. \end{aligned} \tag{21}$$

Similarly to (20), in the slow fading channel, (18) can be further simplified as

$$\widehat{\varphi} \approx \begin{cases} \dfrac{Im\,(Y)}{|h|^2}, \\ if\ \ Re\,(Y) > 0\ and\ \ |Re\,(Y)| \geq |Im\,(Y)| \\ \dfrac{\pi}{2} - \dfrac{Re\,(Y)}{|h|^2}, \\ if\ Im\,(Y) > 0\ and\ \ |Re\,(Y)| < |Im\,(Y)| \\ -\pi - \dfrac{Im\,(Y)}{|h|^2}, \\ if\ \ Re\,(Y) < 0\ and\ \ |Re\,(Y)| \geq |Im\,(Y)| \\ -\dfrac{\pi}{2} + \dfrac{Re\,(Y)}{|h|^2}, \\ if\ Im\,(Y) < 0\ and\ \ |Re\,(Y)| < |Im\,(Y)|\,. \end{cases} \tag{22}$$

After that, with the simplified estimator in (17), (20) and (22), the CFO of the chip sampling value $r_{m,k}$ in (1) can be compensated by

$$r'_{m,k} = r_{m,k} e^{-jk\widehat{\varphi}}. \tag{23}$$

Finally, the detection operation is performed by

$$\widehat{A}\,[m] = \underset{0\leq n\leq 15}{arg\,\max}\left\{A_{m,n}\right\}, \tag{24}$$

where the metric $A_{m,n}$ given by

$$A_{m,n} = \left|\sum_{k=1}^{L_1} r'_{m,k} s^*_{n,k}\right|^2, \quad 0 \leq n \leq 15. \tag{25}$$

Here, L_1 is the number of sample for each symbol in actual data, and $2 \leq L_1 \leq K/2$. The final bit output data $E\,[m]$ can be obtained by symbol demapper. Fig. 3 is the detailed structure of our proposed detector, which processes the output sequence $r_{m,k}$ in Fig. 1.

In this work, a heuristic approach is adopted. First, the CFOE is estimated and compensated under the data-aided configuration. With the compensated signal in (23), the conventional noncoherent detection scheme is followed and extended under spread spectrum. The proposed scheme greatly reduces the complexity and packet error rate due to the simplified but reliable estimator and not performing

TABLE 2. Comparison of hardware complexity.

	Proposed scheme			Coherent detection-based scheme	Conventional noncoherent scheme
	Frequency offset estimator	Frequency offset compensator	Correlator		
Number of adder	6	2	32	60	144
Number of multiplier	12	4	64	120	288

chip-level delay operation. The Algorithm 3 summarizes the specific process of our proposed detection scheme.

algorithm 3

V. NUMERICAL RESULTS AND DISCUSSION

In this section, we evaluate the packet error rate (PER) performance of various detection schemes over the pure AWGN channel and the slow Rayleigh fading channel, which is the common performance index to measure the quality of physical layer data communication. Note that, the physical layer protocol data unit (PPDU) is set to 22 bytes in simulation. For different detectors, the transmitter will repeat sending random packets to the detector for detection until enough error packets are collected. We choose the 2.45 GHz band maximum as the carrier frequency, that is 2.48 GHz. The detailed simulation parameters in this work are shown in Table 2.

A. PERFORMANCE EFFECT OF THE PREAMBLE NUMBER J_1

Increasing the number of preamble can effectively improve the O-QPSK receiver performance. As shown in Fig. 4 (a)-(c), under different number of preambles, we compare the PER performance of our proposed full estimator and two simplified estimators in (32, 4)-DSSS system. The CFO f is considered to rang from -80 to 80 ppm with symmetric triangular distribution, and the CPO θ follows the uniform distribution in $(-\pi, \pi)$. J_1 is the preamble number. We observe from Fig. 4 that PER performance improves as J_1 increases from 1 to 8, but this performance improvement degrades rapidly. Specifically, as shown in Fig. 4 (a), for the PER performance at 1×10^{-3}, as the number of the preamble symbol J_1 increases from 1 to 2, the gain of the SNR is about 1.5 dB; as J_1 increases from 2 to 4, the SNR gain is 1.2 dB; when J_1 is further increased from 4 to 5, the SNR gain is only reduced by 0.2 dB. Further, it can be concluded that the 4 preambles are enough to meet the receiver performance requirement.

In order to observe the performance comparison more clearly, we give performance curves of different estimation algorithms when $J_1 = 1, 4, 8$ in Fig. 5. We can observe from Fig. 5 that the performances of the simplified estimator in (17) and (20) are comparable to that of the full estimator. Actually, according to the performance requirements in different application, we can set appropriate number of the preamble, which provides much higher degree of freedom. Yet, for acquiring

Algorithm 3: The Proposed Detection Algorithm

Input: $r_{m,k}$: baseband samples of the mth symbol period $E[m]$;
L: payload length of the PPDU (here, $L = 176$ bits, *i.e.* 44 symbols);
L_1: sample number for each symbol of the actual data, and $2 \le L_1 \le K/2$;
L_2: sample number for the mth symbol of the preamble, and $2 \le L_2 \le K/2$;
K: chip length of the pseudo-random sequence (PN), and $K = 32$;
N: the number of differential chip, and $N \in \{1, 2, 3\}$;
J_1: the length of preamble, and $1 \le J_1 \le J$, where $J = 8$ is the maximum length.
Output: $\{\widehat{E}[m]\}$: the actual bit data.

Initialize $L = 176$, $K = 32$, and $N = 1$;
for $k = 2;\ k \le L_2;\ k++$ **do**
  $Ds_{0,k-1} \leftarrow s_{0,k} s^*_{0,k-1}$;
end
for $m = 1;\ m \le J_1;\ m++$ **do**
  for $k = 2;\ k \le L_2;\ k++$ **do**
    $Dr_{m,k-1} \leftarrow r_{m,k} r^*_{m,k-1}$;
    $Y \leftarrow Y + Dr_{m,k-1} Ds^*_{0,k-1}$;
  end
end
$Y \leftarrow Y/J_1\,(L_2 - 1)$;
Calculate quantization function $g(Y)$, and $\widehat{\varphi} \triangleq \omega T_c = g(Y)$;
for $m = J_1 + 1;\ m \le J_1 + L/4;\ m++$ **do**
  for $n = 0;\ n \le 15;\ n++$ **do**
    for $k = 1;\ k \le L_1;\ k++$ **do**
      $r'_{m,k} \leftarrow r_{m,k} e^{-jk\widehat{\varphi}}$;
      $A_{m,n} \leftarrow A_{m,n} + r'_{m,k} s^*_{n,k}$;
    end
    $A_{m,n} \leftarrow |A_{m,n}|^2$;
  end
end
for $n = 0;\ n \le 15;\ n++$ **do**
  $\widehat{A}[m] \leftarrow \underset{0 \le n \le 15}{arg\max} \{A_{m,n}\}$;
end
Obtain the bit detection information $\{\widehat{E}[m]\}$ by demapping the output value of the comparator $\{V_m\}$;
return $\{\widehat{E}[m]\}$.

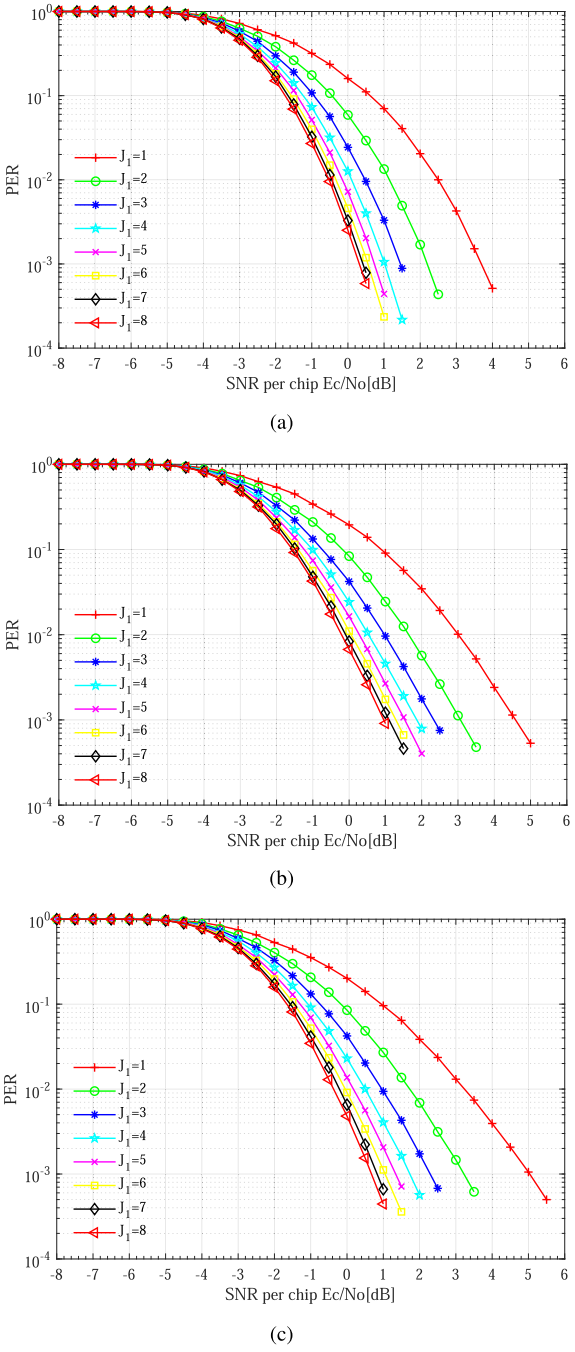

FIGURE 4. Detection performance impact of parameter J_1 under the proposed scheme with different estimators in (32, 4)-DSSS system over pure AWGN channel. (a) PER performance with full estimator in (15); (b) PER performance with simplified estimator in (17); (c) PER performance with simplified estimator in (20).

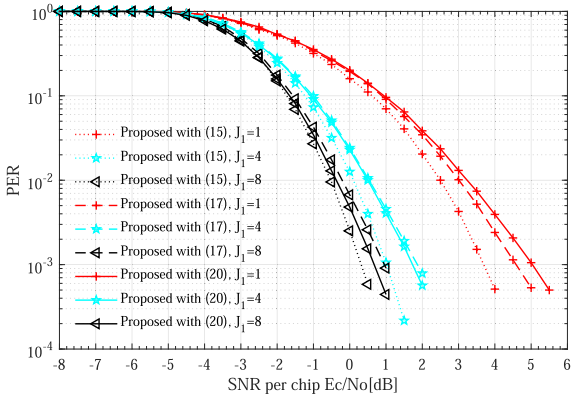

FIGURE 5. Detection performance impact of parameter J_1 under the proposed scheme with different estimators in (32, 4)-DSSS system over pure AWGN channel.

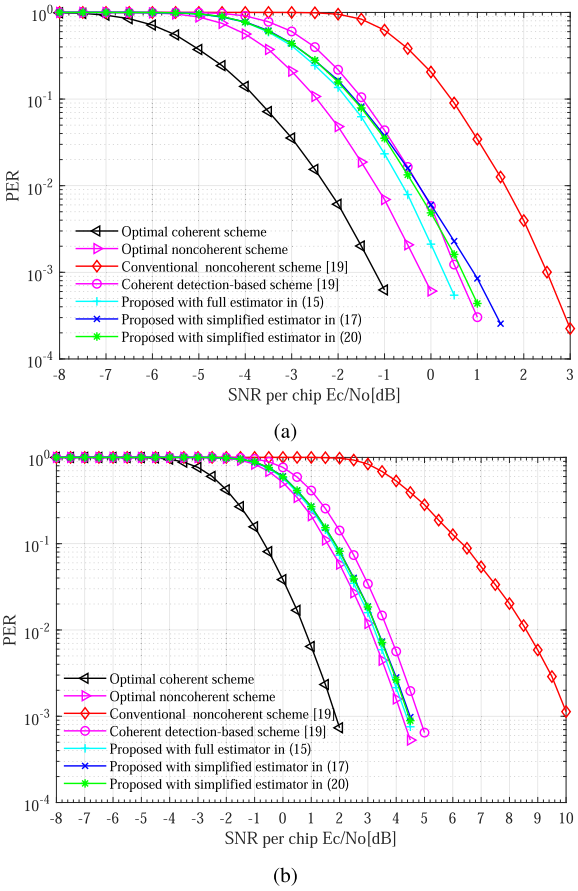

FIGURE 6. Detection performance comparisons of various detection schemes over pure AWGN channel. (a) (32, 4)-DSSS system; (b) (16, 4)-DSSS system.

optimum performance, we consider the maximum truncation factor, *i.e.*, $J_1 = 8$.

B. DETECTION PERFORMANCE ANALYSIS OVER PURE AWGN CHANNEL

Fig. 6 is the PER performance comparison of our proposed scheme with the conventional noncoherent scheme and the 3-chip delay coherent-based scheme [19]. As observed from Fig. 6 (a) and (b), in contrast with the conventional noncoherent scheme, the PER performance of our proposed scheme has been significantly improved. At the PER of 1×10^{-3} in Fig. 6 (a), compared with the conventional noncoherent detection scheme, our proposed full detector acquires almost

2.2 dB gains. Moreover, the performance loss of our proposed simplified detector is also smaller than that of the full estimator, meanwhile it also possesses lower complexity. In addition, we can also observe from Fig. 6 (a) that in the (32, 4)-DSSS system, the PER performance of our proposed simplified detector is close to the coherent-based scheme in [19], and yet our detector provide a lower complexity.

According to the IEEE 802.15.4 WSNs standard, the modulation method using O-QPSK DSSS has three different spreading modes, including (32, 4)-DSSS, (16, 4)-DSSS and (8, 4)-DSSS. This section also verifies the PER performance of (16, 4)-DSSS system, and we can observe form Fig. 6 (b) that the proposed scheme shows well performance in (16, 4)-DSSS system. Particularly, at the PER of 1×10^{-3}, in contrast with the conventional noncoherent detection scheme, the proposed simplified estimation scheme achieves 5.6 dB gain, which shows a higher gain than the (32, 4)-DSSS system. Furthermore, the performance of the two simplified estimators and full estimator implemented in (16, 4)-DSSS system is similar to that in (32, 4)-DSSS system. Therefore, the proposed detection scheme is also applicable to the (16, 4)-DSSS system and has better performance than the (32, 4)-DSSS system. Keep these discussions in mind, we conclude boldly that the detection scheme proposed in this work is also applicable in (8, 4)-DSSS system, but detailed verification is not performed here.

C. DETECTION PERFORMANCE ANALYSIS OVER SLOW FADING CHANNEL

Fig. 7 is the detection performance comparisons of various schemes in (32,4)-DSSS and (16,4)-DSSS systems, respectively. As shown in Fig. 7, under the slow Rayleigh fading channel with normalized average power, the performance of our proposed receiver has been investigated in the (32,4)-DSSS and (16,4)-DSSS systems. We can observe from Fig. 7 that there is a small performance degradation between the full estimation and simplified estimator. That is to say, in the normalized slow fading channel, the complexity of our detector is reduced, but no large performance degradation is observed. In particular, as shown in Fig. 7 (a), at PER of 1×10^{-2}, compared with the conventional noncoherent scheme in [19], our proposed simplified scheme achieves 2.5 dB and 4.5 dB gains in (32,4)-DSSS system and (16,4)-DSSS system, respectively. Further, the performance of our detector is close to the coherent scheme in [19], which is also observed under the AWGN channel as shown in Fig. 6.

D. ROBUSTNESS OF THE RECEIVER

The PER performance of our proposed scheme under various dynamic CFO in the $(32, 4)$ $-$DSSS system is shown in Fig. 8. It is considered that CPO θ follows the uniform distribution from $-\pi$ to π. The horizontal black dashed line represents the proposed full estimator given in (15), which provides a baseline for comparison. Moreover, the blue solid line describes proposed simplified estimator performance given in (17), where involves $\tan^{-1}(x) \approx x$; the green solid line

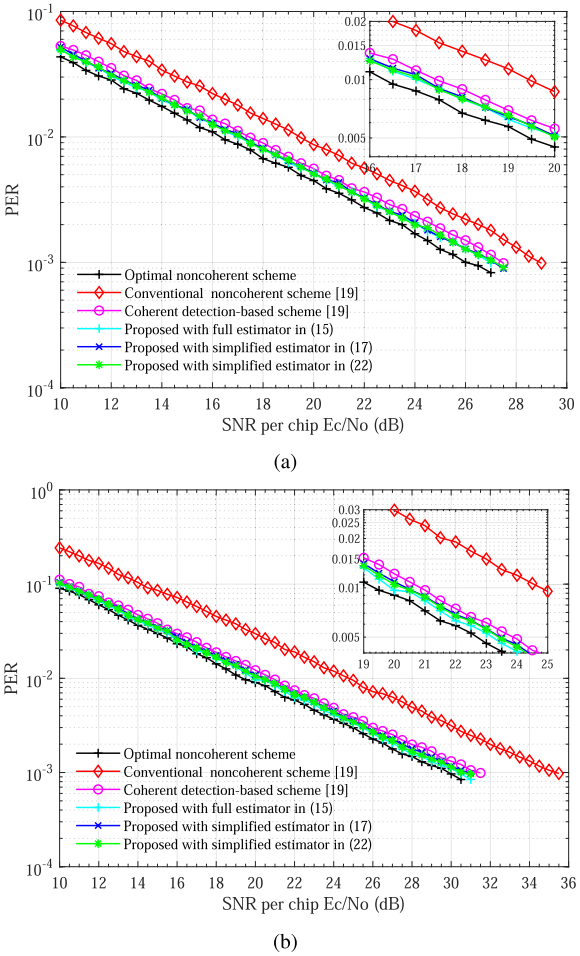

FIGURE 7. Detection performance comparisons of various detection schemes under the normalized slow Rayleigh fading channel. (a) (32, 4)-DSSS system; (b) (16, 4)-DSSS system.

depicts the performance of proposed simplified estimator given in (21), where $\sin^{-1}(x) \approx x$ and $|Y| \approx 1$ are involved.

We can observe from Fig. 8 that, when the CFOE is between $+20$ and -20 ppm, the PER performance is well; when the CFOE is greater than $+20$ ppm or less than -20 ppm, the PER performance is severely impaired. In particular, from Fig. 8 (a), we can see that when SNR$= -6$, the performance of the three algorithms almost overlap; when SNR$= -4$, the performance of the three algorithms we propose is comparable Close. As shown in in Fig. 8 (b), as the SNR increases, the PER performance suffers more severely. This is mainly because, the absolute estimation error is gradually approaching its maximum value. Yet, when our detection scheme only considers CPO (*i.e.*, without CFO), it offers much less gain than our detector for all CFOs. Hence, the augmented detector in this work is not sensitive to frequency offset.

E. PERFORMANCE UNDER UNDER DYNAMIC PHASE CHANNEL

In this subsection, we investigate the detection effect of our proposed receiver when the carrier phase changes from

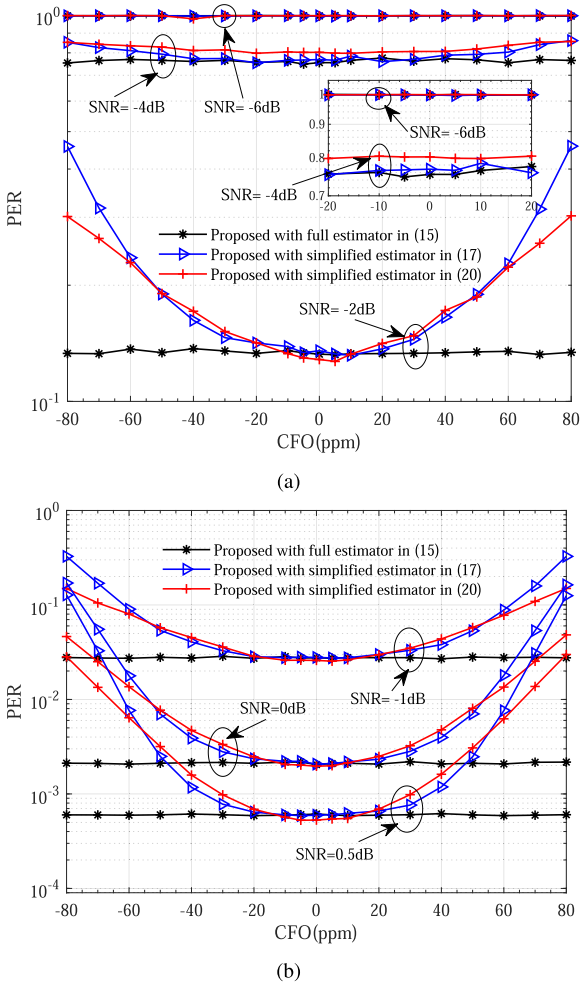

FIGURE 8. Detection performance comparisons of our proposed scheme under various estimators versus CFO in (32, 4)-DSSS system over pure AWGN channel. (a) SNR= −6, −4, −2; (b) SNR=−1, 0, 0.5.

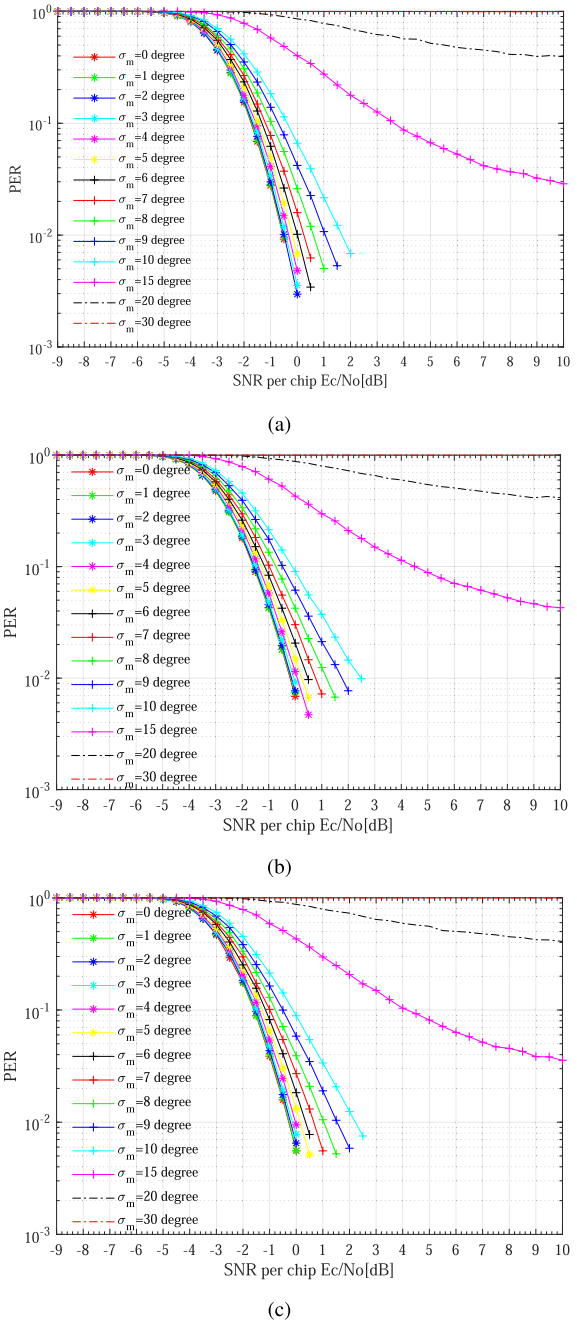

FIGURE 9. Detection performance comparison of our proposed scheme versus dynamic CPO in (32, 4)-DSSS system over pure AWGN channel. (a) PER performance with full estimator in (15); (b) PER performance with simplified estimator in (17); (c) PER performance with simplified estimator in (20).

symbol to symbol. Fig. 9 (a)-(c) respectively shows the relationship between PER performance and dynamic CPO of the proposed detection scheme under different estimation algorithms. The phase θ is modeled as the Wiener process $\theta_{m+1} = \theta_m + \Delta_m$, where Δ_m is a zero-mean Gaussian random variable independent of the known variance σ_m^2 at each symbol interval. The initial phase θ_1 follows a uniform distribution in $(-\pi, \pi)$. As shown in Fig. 9 (a), it is clear that our noncoherent detection scheme is robust to phase jitter, and increasing the standard deviation of the jitter to 5 degrees will not significantly reduce the performance of our proposed receiver. Moreover, it can also be observed that as the SNR increases, different estimation algorithms all show an irreducible level of error.

We further compare the performance of our proposed scheme with different estimation algorithms under dynamic phase channel in Fig. 10. As shown in Fig. 10, our proposed scheme with the full estimator can provides more robustness to the CPO, and the simplified estimators in (17) and (20) greatly reduces the complexity of implementation but with a small performance cost. In particular, as the standard deviation reduces, the influence of the phasor $e^{j\Delta_m}$ on the correlator output $A[m]$ will be lesser and lesser. This is mainly because the random phase increment $e^{j\Delta_m}$ produces a phasor in the correlator output $A[m]$.

F. COMPUTATIONAL COMPLEXITY

Finally, the hardware complexity of various detection schemes are investigated from the perspective of the number

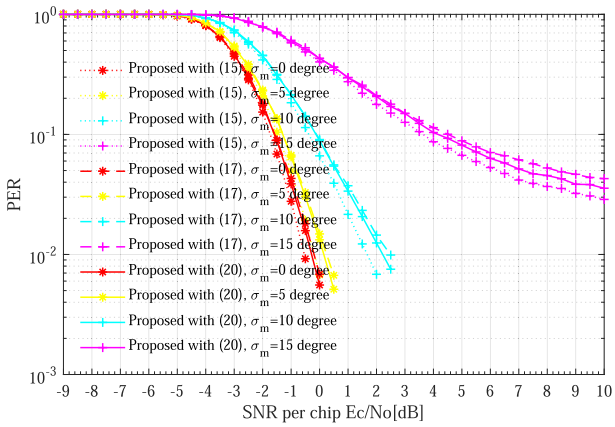

FIGURE 10. Detection performance comparison of our proposed scheme with different estimators versus dynamic CPO in (32, 4)-DSSS system over pure AWGN channel.

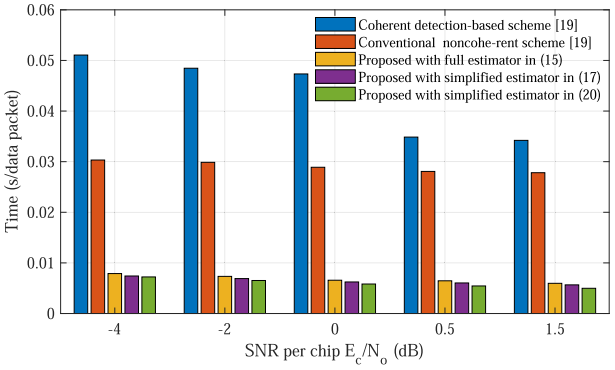

FIGURE 11. Comparisons of average running time per data packet under various detection schemes in (32, 4)-DSSS system over pure AWGN channel.

of adders and multipliers. Table 2 shows the complexity comparison of our proposed scheme and the existing detection schemes. Note that, as shown in Fig. 2, we record the process of multiplying two complex conjugates as two adders and four multipliers. As shown in Table 2, our proposed detector consumes only 40 adders and 80 multipliers. The 3-chip delay coherent-based detector in [19] contains 60 adders and 120 multipliers, which is 1.5 times the scheme we proposed; the conventional noncoherent detector in [19] contains 144 adders and 288 multipliers, this is 3.6 times that of our proposed scheme. Obviously, the hardware complexity of our proposed scheme has been significantly reduced compared to the other two.

Furthermore, our proposed detection scheme also possess lower computational complexity, which will be analyzed from the perspective of average running time. Specifically, we simulated the running time of the same number of transmission packets under different detection schemes. Note that, we run 10^5 data packets under different detection schemes, and then calculate their average running time of each data packet. We can observe from Fig. 11 that the packet running time of our proposed scheme in this work is significantly lower than that of other schemes. As the SNR increases, the data packet running time of each scheme decreases, which is mainly due to the reduction of the packet error rate and the improvement of detection performance. Specifically speaking, as illustrated in Fig. 11, for the SNR of 0.5 dB, the average running time per packet under our proposed full estimation scheme is 0.59×10^{-2} s, while the conventional noncoherent scheme in [19] is 0.28×10^{-1} s, which is 4.7 times of our proposed scheme; and the coherent-based scheme in [19] is 0.34×10^{-1} s, which is 5.8 times of our proposed scheme. Obviously, the average running time per packet in our proposed scheme has been significantly reduced, which is expected by low-power and low-cost WSNs nodes.

VI. CONCLUSION AND FUTURE WORK

We have put forward an implementation-friendly and energy-efficient noncoherent detection scheme for IEEE 802.15.4 O-QPSK receivers. In this configuration, the CFO is estimated and compensated. Experimental results show that, with the assist of only four preambles, our detection performance meets the requirements of IEEE WSNs. Also, when the standard deviation of phase jitter is up to 5 degrees, it will not significantly reduce receiver performance. Finally, compared to conventional noncoherent scheme in [19], our enhanced scheme perform more attractive in terms of complexity and reliability. Hence, the proposed detection strategy is more reasonable for O-QPSK receivers, whose representative application fields are wireless body area networks, smart grids and home automation.

Furthermore, there are some future investigate directions. The first is that the full multi-symbol detection scheme can be easily inferred based on the existing framework, wherein the observation interval is allowed to be two symbols or more [26]. The application of this detection scheme can further narrow the performance gap between ideal coherent detection and optimal noncoherent detection [27]. Second, technologies with reduced complexity can be developed for the full multi-symbol detection [28], [29]. Low-complexity algorithms benefit less energy consumption, which is obviously desirable in the design of battery-powered receivers. Finally, combining O-QPSK with channel coding is expected to provide higher reliability, and iterative noncoherent detection is desired [30]. These work will be reported by the author in an upcoming paper.

REFERENCES

[1] W. Shi, J. Cao, Q. Zhang, Y. Li, and L. Xu, "Edge computing: Vision and challenges," *IEEE Internet Things J.*, vol. 3, no. 5, pp. 637–646, Oct. 2016.

[2] W. Yu, F. Liang, X. He, W. Grant Hatcher, C. Lu, J. Lin, and X. Yang, "A survey on the edge computing for the Internet of Things," *IEEE Access*, vol. 6, pp. 6900–6919, 2018.

[3] J. Gubbi, R. Buyya, S. Marusic, and M. Palaniswami, "Internet of Things (IoT): A vision, architectural elements, and future directions," *Future Gener. Comput. Syst.*, vol. 29, no. 7, pp. 1645–1660, Sep. 2013.

[4] *IEEE Standard for Low-Rate Wireless Networks*, IEEE Standard 802.15.4-2015, IEEE Press, New York, NY, USA, 2016.

[5] *Information Technology–Telecommunications and Information Exchange Between Systems-Local and Metropolitan Area Networks–Specific Requirements-Part 15-4: Wireless Medium Access Control (MAC) and Physical Layer (PHY) Specifications for Low-Rate Wireless Personal Area Networks (WPANs)*, ISO/IEC/IEEE Standard 802.15.4-2018, IEEE Press, New York, NY, USA, 2018.
[6] S. M. Kay, *Fundamentals of Statistical Signal Processing: Detection Theory*. Upper Saddle River, NJ, USA: Prentice-Hall, 1998, pp. 563–596.
[7] X. Li, J. Li, Y. Liu, Z. Ding, and A. Nallanathan, "Residual transceiver hardware impairments on cooperative NOMA networks," *IEEE Trans. Wireless Commun.*, vol. 19, no. 1, pp. 680–695, Jan. 2020.
[8] X. Li, J. Li, and L. Li, "Performance analysis of impaired SWIPT NOMA relaying networks over imperfect Weibull channels," *IEEE Syst. J.*, vol. 14, no. 1, pp. 669–672, Mar. 2020.
[9] M. Zhan, J. Wu, H. Wen, and P. Zhang, "A novel error correction mechanism for energy-efficient cyber-physical systems in smart building," *IEEE Access*, vol. 6, pp. 39037–39045, 2018.
[10] M. Zhan, Z. Pang, D. Dzung, and M. Xiao, "Channel coding for high performance wireless control in critical applications: Survey and analysis," *IEEE Access*, vol. 6, pp. 29648–29664, 2018.
[11] H. Harada, K. Mizutani, J. Fujiwara, K. Mochizuki, K. Obata, and R. Okumura, "IEEE 802.15.4G based Wi-SUN communication systems," *IEICE Trans. Commun.*, vol. E100.B, no. 7, pp. 1032–1043, 2017.
[12] L. Underberg, R. Croonenbroeck, A. Wulf, W. Endemann, and R. Kays, "A PSSS approach for wireless industrial communication applying iterative symbol detection," *IEEE Trans. Ind. Informat.*, vol. 14, no. 5, pp. 2108–2119, May 2018.
[13] S. Fang, S. Berber, A. Swain, and S. U. Rehman, "A study on DSSS transceivers using OQPSK modulation by IEEE 802.15.4 in AWGN and flat Rayleigh fading channels," in *Proc. IEEE Region Conf. (TENCON)*, Jan. 2010, pp. 1347–1351.
[14] S. J. Savory, "Digital coherent optical receivers: Algorithms and subsystems," *IEEE J. Sel. Topics Quantum Electron.*, vol. 16, no. 5, pp. 1164–1179, Sep. 2010.
[15] S. Park, D. Park, H. Park, and K. Lee, "Low-complexity frequency-offset insensitive detection for orthogonal modulation," *Electron. Lett.*, vol. 41, no. 22, pp. 1226–1228, Oct. 2005.
[16] D. Park, C. S. Park, and K. Lee, "Simple design of detector in the presence of frequency offset for IEEE 802.15.4 LR-WPANs," *IEEE Trans. Circuits Syst. II, Exp. Briefs*, vol. 56, no. 4, pp. 330–334, Apr. 2009.
[17] S. Dai, H. Qian, K. Kang, and W. Xiang, "A robust demodulator for OQPSK–DSSS system," *Circuits, Syst., Signal Process.*, vol. 34, no. 1, pp. 231–247, Jan. 2015.
[18] C. Wang, Y. Liu, R. Luo, and H. Yang, "A low-complexity symbol-level differential detection scheme for IEEE 802.15.4 O-QPSK signals," in *Proc. Int. Conf. Wireless Commun. Signal Process.*, Huangshan, China, Oct. 2012, pp. 1–6.
[19] J.-H. Do, J.-S. Han, H.-J. Choi, U. Lee, and S.-H. Min, "A coherent detection-based symbol detector algorithm for 2.45GHz LR-WPAN receiver," in *Proc. IEEE Region Conf. (TENCON)*, Melbourne, VIC, Australia, Nov. 2005, pp. 1–6.
[20] K.-H. Lin, W.-H. Chiu, and J.-D. Tseng, "Low-complexity architecture of carrier frequency offset estimation and compensation for body area network systems," *Comput. Math. with Appl.*, vol. 64, no. 5, pp. 1400–1408, Sep. 2012.
[21] J.-Y. Oh, B.-J. Kwak, and J.-Y. Kim, "Carrier frequency recovery for in non-coherent demodulation for IEEE802.15.4 system," in *Proc. IEEE Veh. Technol. Conf.*, Melbourne, VIC, Australia, Sep. 2006, pp. 1864–1868.
[22] H.-J. Jeon, T. Demeechai, W.-G. Lee, D.-H. Kim, and T.-G. Chang, "IEEE 802.15.4 BPSK receiver architecture based on a new efficient detection scheme," *IEEE Trans. Signal Process.*, vol. 58, no. 9, pp. 4711–4719, Sep. 2010.
[23] S. Lee, H. Kwon, Y. Jung, and J. Kim, "Efficient non-coherent demodulation scheme for IEEE 802.15.4 LR-WPAN systems," *Electron. Lett.*, vol. 43, no. 16, pp. 879–880, Aug. 2007.
[24] G. Zhang, D. Wang, L. Song, H. Wu, P. Xie, B. Ji, and H. Wen, "Simple non-coherent detection scheme for IEEE 802.15.4 BPSK receivers," *Electron. Lett.*, vol. 53, no. 9, pp. 628–629, Apr. 2017.
[25] G. Zhang, H. Wen, L. Wang, L. Song, J. Tang, and R. Liao, "Simple and robust near-optimal single differential detection scheme for IEEE 802.15.4 BPSK receivers," *IET Commun.*, vol. 13, no. 2, pp. 186–197, Jan. 2019.
[26] B. Li, "A new reduced-complexity algorithm for multiple-symbol differential detection," *IEEE Commun. Lett.*, vol. 7, no. 6, pp. 269–271, Jun. 2003.
[27] G. Zhang, H. Wen, L. Wang, X. Zeng, J. Tang, R. Liao, and L. Song, "Multiple symbol differential detection scheme for IEEE 802.15.4 BPSK receivers," *IEICE Trans. Fundam. Electron., Commun. Comput. Sci.*, vol. E101.A, no. 11, pp. 1975–1979, 2018.
[28] F. Adachi and M. Sawahashi, "Viterbi-decoding differential detection of DPSK," *Electron. Lett.*, vol. 28, no. 23, pp. 2196–2198, Nov. 1992.
[29] K. M. Mackenthun, "A fast algorithm for multiple-symbol differential detection of MPSK," *IEEE Trans. Commun.*, vol. 42, no. 234, pp. 1471–1474, Apr. 1994.
[30] G. Zhang, H. Wen, J. Pu, and J. Tang, "Build-in wiretap channel I with feedback and LDPC codes by soft decision decoding," *IET Commun.*, vol. 11, no. 11, pp. 1808–1814, Aug. 2017.

GAOYUAN ZHANG received the Ph.D. degree from the National Key Laboratory of Communications, University of Electronic Science and Technology of China, Chengdu, China, in 2015. He is currently an Associate Professor with the School of Electronic and Information Engineering, Henan University of Science and Technology. His current research interests include short distance communication, physical layer security, modulation, and error-control coding.

CONGYU SHI was born in Henan, China, in 1996. She received the B.S. degree in electronic information engineering from the Henan University of Science and Technology, China, in 2018, where she is currently pursuing the M.S. degree. Her current research interests include short distance communication and error-control coding.

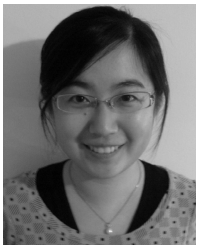

CONGZHENG HAN received the Ph.D. degree in electrical and electronic engineering from the University of Bristol, U.K., in 2008. She worked with the University of Bristol, the Toshiba European Communication Technology Research Laboratory (project cooperation), U.K., the Mobile Communication Virtual Research Center, and the U.K. Telecom Regulatory Authority. Her main research interests include wireless LAN, multi-carrier transmission technology, MIMO, multi-user transmission, wireless resource optimization, opportunistic scheduling algorithms, location information aided communication, green energy saving communication, British and European communication standards, electromagnetic wave energy acquisition and storage technology, and atmospheric observation technology.

XINGWANG LI (Senior Member, IEEE) received the B.Sc. degree from Henan Polytechnic University, in 2007, the M.Sc. degree from the University of Electronic Science and Technology of China, in 2010, and the Ph.D. degree from the Beijing University of Posts and Telecommunications, in 2015.

From 2010 to 2012, he was working at Comba Telecom Ltd., Guangzhou, China, as an Engineer. He spent one year, from 2017 to 2018, as a Visiting Scholar at Queen's University Belfast, Belfast, U.K. He was a Visiting Scholar with the State Key Laboratory of Networking and Switching Technology, Beijing University of Posts and Telecommunications, from 2016 to 2018. He is currently an Associate Professor with the School of Physics and Electronic Information Engineering, Henan Polytechnic University, Jiaozuo, China. His research interests include MIMO communication, mining communication, non-orthogonal multiple access, cooperative communication, hardware constrained communication, physical layer security, unmanned aerial vehicles, and the Internet of Things.

Dr. Li is also an Editor on the Editorial Board of IEEE Access, *Computer Communications*, and the *KSII Transactions on Internet and Information Systems*. He is the Lead Guest Editor of the Special Issue on Recent Advances in Physical Layer Technologies for 5G-Enabled Internet of Things of *Wireless Communications and Mobile Computing*. He has served for many conferences as a TPC member, such as IEEE CIC, IEEE GLOBECOM, and IEEE WCNC. He is also the Co-Chair of the IEEE/IET CSNDSP 2020 of the Green Communications and Networks Track.

DAN WANG received the Ph.D. degree in communication and information systems from Shanghai Jiao Tong University, in 2009. In April 2009, she served as an Associate Professor with the School of Information Engineering, Henan University of Science and Technology. As the first author, she won two first prizes and one second prize in the Henan Province's Tenth Natural Science Excellent Academic Paper Competition. Her research interests include new generation of wireless communication system theory and key technology, and the theory of ultra-wideband wireless communication systems.

KHALED RABIE (Senior Member, IEEE) received the M.Sc. and Ph.D. degrees in electrical and electronic engineering from The University of Manchester, in 2011 and 2015, respectively. He is currently an Assistant Professor with the Department of Engineering, Manchester Metropolitan University (MMU), U.K. He has worked as a part of several large-scale industrial projects and has published more than 100 journal and conference papers (mostly IEEE). His primary research interest includes next-generation wireless communication systems. He is also a Fellow of the U.K. Higher Education Academy (FHEA). He has received numerous awards over the past few years in recognition of his research contributions, including the Best Student Paper Award at IEEE ISPLC, TX, USA, in 2015; the MMU Outstanding Knowledge Exchange Project Award, in 2016; and IEEE Access Editor of the Month Award, in August 2019. He serves regularly for the Technical Program Committee (TPC) of several major IEEE conferences, such as GLOBECOM, ICC, and VTC. He serves as an Editor for the IEEE Communications Letters, an Associate Editor for IEEE Access, an Area Editor for *Physical Communication*, and an Executive Editor for the *Transactions on Emerging Telecommunications Technologies*.

RUPAK KHAREL (Senior Member, IEEE) received the Ph.D. degree in secure communication systems from Northumbria University, U.K., in 2011. He is currently a Reader (an Associate Professor) with the Department of Computing and Mathematics, Manchester Metropolitan University. His research interests include various use cases and the challenges of the IoT and cyber physical systems, including the Internet of Vehicles (IoV), cyber security, physical layer security, 5G, and beyond systems. He is a member of IET and a Fellow of the Higher Education Academy (FHEA), U.K. He is a Principal Investigator of multiple government and industry funded research projects.